CrossMark

J. Fluid Mech. (2023), *vol*. 959, A1, doi:10.1017/jfm.2023.52

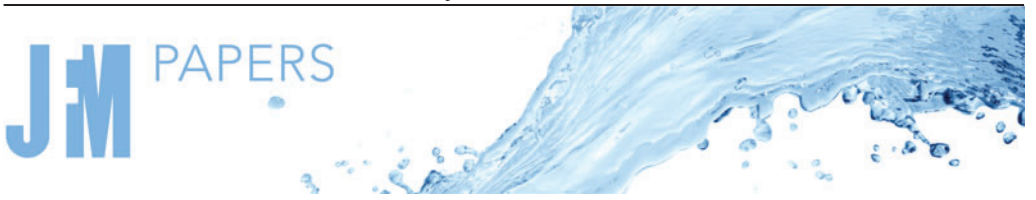

Complex-network analysis of high-frequency combustion instability in a model single-element rocket engine combustor

Kazuki Kawano[1], Hiroshi Gotoda[1],†, Yusuke Nabae[1], Yuya Ohmichi[2] and Shingo Matsuyama[2],†

[1]Department of Mechanical Engineering, Tokyo University of Science, 6-3-1 Niijuku, Katsushika-ku, Tokyo 125-8585, Japan

[2]Japan Aerospace Exploration Agency, 7-44-1 Jindaiji-Higashimachi, Chofu-shi, Tokyo 182-8522, Japan

(Received 12 June 2022; revised 12 November 2022; accepted 22 December 2022)

We study the spatio-temporal dynamics of high-frequency combustion instability in a model single-element rocket combustor using an acoustic energy flux-based spatial network. The acoustic energy source collapses by the formation of small communities with weak connection when the flame edge is attached to the injector rim. In contrast, large communities with strong connection are formed in the shear layer between the oxygen and hydrogen jets when the flame edge is detached from the injector rim, which has a significant impact on driving combustion instability. The switching between the attachment and detachment of the flame edge during combustion instability can be explained by the spectral-clustering-based transition network constructed from the pressure and flow velocity of the hydrogen jet at the injector exit, and the temperature near the injector rim.

Key words: combustion, turbulent reacting flows

1. Introduction

Combustion instability is the amplification phenomenon of thermoacoustic resonance modes and is sustained by the feedback mechanisms coupling mutually among the fluctuations in pressure, heat release and hydrodynamics in wide-ranging combustors including power plants and aircraft and rocket engines. It is classified by acoustic pressure fluctuations inside a combustor into three combustion instabilities, on the basis of the range of the dominant frequencies in the combustor: low-frequency (<50 Hz), intermediate-frequency (50–1000 Hz), and high-frequency (>1000 Hz) combustion

† Email addresses for correspondence: gotoda@rs.tus.ac.jp, matsuyama.shingo@jaxa.jp

© The Author(s), 2023. Published by Cambridge University Press

https://doi.org/10.1017/jfm.2023.52 Published online by Cambridge University Press

instabilities (Lieuwen & Yang 2005). The incidence of combustion instability generates mechanical vibrations of the combustor and the increase in the heat transfer rate to the combustor wall, shortening the lifetime and causing serious structural damage to combustors. Extensive and comprehensive reviews on the feedback mechanisms have been provided by Lieuwen & Yang (2005), Huang & Yang (2009), Lieuwen (2012) and O'Connor, Acharya & Lieuwen (2015). Many numerical and experimental investigations on high-frequency combustion instability in various model rocket engine combustors have focused on the following points related to the driving and feedback mechanisms: (i) the coupling of pressure and heat release rate fluctuations (Armbruster, Hardi & Oschwald 2021), (ii) the mutual interaction between the acoustic modes inside the combustor and the oxygen injector (Gröning *et al.* 2016; Urbano *et al.* 2016; Martin *et al.* 2021), (iii) the induction of fuel flow velocity fluctuations due to the propagation of pressure fluctuations into the fuel injector (Urbano *et al.* 2017), (iv) the effects of the pressure and flow velocity fluctuations on the jet flame behaviour (Morgan, Shipley & Anderson 2015) and (v) the driving of high-frequency combustion instability due to a repetition of detachment and reignition of a jet flame at the shear layer region between fuel and oxidizer flows (Harvazinski *et al.* 2015).

The complex-network approach (Newman 2010; Barabási 2016) inspired by discrete mathematics has recently enabled us to clarify the nonlinear dynamics of intermediate-frequency combustion instability in several turbulent combustors (Murugesan & Sujith 2015; Okuno, Small & Gotoda 2015; Godavarthi *et al.* 2018; Murayama *et al.* 2018; Guan *et al.* 2019; Kobayashi *et al.* 2019; Krishnan *et al.* 2019*b*, 2021). The importance of the complex-network approach in the fields of combustion engineering and fluid physics has been shown in some recent review articles (Juniper & Sujith 2018; Sujith & Unni 2020, 2021; Iacobello, Ridolfi & Scarsoglio 2021) and a book (Sujith & Pawar 2021). These works have proactively adopted a wide variety of complex networks such as the visibility graph (Lacasa *et al.* 2008; Lacasa & Toral 2010), the turbulence network (Taira, Nair & Brunton 2016), the cycle network (Zhang & Small 2006), the ordinal partition transition network (McCullough *et al.* 2015; Zhang *et al.* 2017), a recurrence network (Marwan *et al.* 2007) and a spatial network (Iacobello *et al.* 2021) for revealing the nonlinear dynamics during a transitional state from combustion noise to intermediate-frequency combustion instability. One of the most promising networks used to clarify the spatio-temporal dynamics of combustion instability is the spatial network (e.g. an acoustic power network) (Krishnan *et al.* 2019*b*). Krishnan *et al.* (2019*b*) studied the spatio-temporal dynamics of combustion noise and combustion instability in a bluff-body-stabilized combustor using a weighted acoustic power network. They elucidated that the acoustic power sources emerge as fragmented clusters during combustion noise, whereas large clusters of acoustic power sources are formed during intermediate-frequency combustion instability.

Regarding high-frequency combustion instability in a model rocket combustor, we have recently conducted two studies (Hashimoto *et al.* 2019; Shima *et al.* 2021) on the spatio-temporal dynamics of combustion instability in a cylindrical combustor with an off-centre-installed coaxial injector, including the feedback mechanism in the transitional state to combustion instability. Hashimoto *et al.* (2019) showed that a scale-free structure in the turbulence network is largely maintained during combustion instability. They also showed that the transfer entropy (Schreiber 2000) is valid for determining the directional dependence between the pressure and heat release rate fluctuations that is strongly associated with the feedback mechanisms in the onset of combustion instability. Shima *et al.* (2021) clarified that the flow velocity fluctuations in the fuel injector play an

https://doi.org/10.1017/jfm.2023.52 Published online by Cambridge University Press

important role in the large fluctuations of the heat release rate by estimating the symbolic transfer entropy (Staniek & Lehnertz 2008). They also elucidated that the emergence and collapse of the clusters in an unweighted acoustic power network occur periodically with the generation of combustion instability. Aoki *et al.* (2020) experimentally examined the randomness of pressure fluctuations during intermittent high-frequency combustion instability in a cylindrical combustor by estimating the information entropy in an ordinal partition transition network. Koizumi *et al.* (2020) examined the directional coupling between the pressure and heat release rate fluctuations during high-frequency combustion instability in a continuously variable resonance combustor using the transfer entropy. Kasthuri *et al.* (2022) have experimentally studied the spatio-temporal dynamics during a transition from the intermittent state to high-frequency combustion instability in a model rocket combustor with multiple elements using a weighted spatial network.

A machine learning approach based on statistical learning theory (Bishop 2006) has recently attracted considerable attention in all scientific disciplines and is highly expected to lead to an in-depth understanding of complex nonlinear combustion dynamics and the development of sophisticated detectors of a precursor of combustion instability (Hachijo *et al.* 2019; Kobayashi *et al.* 2019; Shinchi *et al.* 2021; Waxenegger-Wilfing *et al.* 2021; Guan *et al.* 2022). Gotoda and co-workers (Hachijo *et al.* 2019; Kobayashi *et al.* 2019) attempted to detect a precursor of intermediate-frequency combustion instability in a swirl-stabilized combustor using a combinational methodology of the ordinal partition transition network or Jensen–Shannon complexity–entropy causality plane (Rosso *et al.* 2007), *k*-means clustering (Lloyd 1982) and a support vector machine (Vapnik 1999). The early detection of combustion instability in a staged multisector combustor (Shinchi *et al.* 2021) and a cryogenic rocket thrust chamber (Waxenegger-Wilfing *et al.* 2021) has more recently been examined, both of which consider recurrence-based analysis (Marwan *et al.* 2007) and the support vector machine. Guan *et al.* (2022) elucidated the relationship between the two interactions: pressure–pressure and pressure–heat release rate interactions during intermediate-frequency combustion instability in coupled swirl-stabilized combustors using a combinational methodology of the joint recurrence network (Marwan *et al.* 2007) and Gaussian mixture model clustering (Reynolds 2009).

As mentioned above, the formation and feedback mechanisms of high-frequency combustion instability have been examined in many experimental and numerical studies (Harvazinski *et al.* 2015; Morgan *et al.* 2015; Gröning *et al.* 2016; Urbano *et al.* 2016, 2017; Armbruster *et al.* 2021; Martin *et al.* 2021). However, in those studies, the relevance of the interesting switching phenomena between the attached and lifted flame edges from the injector to the sustainment mechanism of high-frequency combustion instability has not been investigated from the viewpoint of complex networks and machine learning. The main aim of this study is to extend our understanding of the sustainment mechanism of high-frequency combustion instability in a model single-element rocket combustor, focusing mainly on the community detection of complex networks and machine learning. Research groups conducting recent studies (Aoki *et al.* 2017; Urbano & Selle 2017) on the driving region of combustion instability evaluated the energy budget of acoustic power production during combustion instability by disturbance energy analysis (Brear *et al.* 2012) in terms of the Rayleigh index. In this study, we first propose a local Rayleigh index ratio consisting of the heat release rate and molecular production terms. As mentioned above, Shima *et al.* (2021) proposed an unweighted acoustic power network consisting of the product of the pressure and heat release rate fluctuations. They captured the emergence of a thermoacoustic cluster during a transitional state to high-frequency combustion instability by calculating only the sign of the products of the pressure and

https://doi.org/10.1017/jfm.2023.52 Published online by Cambridge University Press

heat release rate fluctuations. Their network can successfully extract the periodic change in the cluster coefficient in response to the pressure fluctuations, but it remains difficult to sufficiently explain the fast switching phenomena between the attached and lifted flame edges from the injector during high-frequency combustion instability. Their network does not particularly fail to extract the thermoacoustic damping source in the acoustic power network. Therefore, a more advanced spatial network from the viewpoint of acoustic energy flux in the acoustic energy equation should be taken into account to appropriately deal with such switching phenomena during combustion instability. To this end, we newly propose a class of spatial network different from that developed in the previous studies (Shima *et al.* 2021), namely, an acoustic energy flux-based spatial network. The division of network nodes into groups (community) with dense/sparse connections is an important approach for the reduction or coarse graining of networks (Newman 2010). The *P–Z* map (Guimerà & Amaral 2005) is a useful tool for identifying the role of nodes in terms of community and has recently been adopted to examine the dynamic behaviour of turbulent flows (Meena & Taira 2021). Nevertheless, the community detection has not been adopted in previous studies on high-frequency combustion instability in a model rocket engine combustor, except for intermediate-frequency combustion instability in a swirl-stabilized turbulent combustor (Murayama *et al.* 2018). In this study, we adopt the *P–Z* map for the acoustic energy flux-based spatial network. We finally introduce a clustering-based transition network using the spectral-clustering method (Von Luxburg 2007) in terms of machine learning. Note that, similarly to the motivation of Guan *et al.* (2022), we employ spectral clustering as unsupervised machine learning to reveal the hidden network dynamics of unlabelled physical quantities (pressure, flow velocity of the fuel jet and temperature) associated with the feedback mechanism of high-frequency combustion instability in our combustor, rather than to detect a precursor of combustion instability using a new data set.

This paper comprises four sections. Section 2 gives the framework of the analytical methods, including a brief description of the numerical computation. Results and discussion are presented in § 3. The findings obtained in this study are summarized in § 4.

2. Analytical method

Matsuyama *et al.* (2016) computationally obtained the spatio-temporal combustion field during a transitional state and the subsequent high-frequency combustion instability by high-resolution large-eddy simulation. In this study, we adopt the following analytical methods for the spatio-temporal data (Matsuyama *et al.* 2016). Details of the computation, including the governing equations, the numerical scheme and the initial and boundary conditions, are described by Matsuyama *et al.* (2016).

The model rocket engine combustor that we employed in this study comprises a cylindrical combustor with an off-centre-installed coaxial injector. The H_2/O_2 injector is set at $y = 72$ mm from the centre of the combustor, where y is the transverse direction of the combustor. Here, H_2 and O_2 are respectively released from the outer and inner injectors. The outer (inner) diameter of the H_2 (O_2) injector rim is 8.6 mm (4.9 mm). The first tangential (1 T)-mode oscillations with approximately 1 kHz, which exceed $\pm 3\,\%$ of the time-averaged pressure in the combustor, are clearly produced by their computation (figure 1*a*). The flame dynamics during combustion instability switches back and forth between the attached and lifted flame edges from the injector rim, with accompanying large-scale organized vortex rings (Matsuyama *et al.* 2016;

https://doi.org/10.1017/jfm.2023.52 Published online by Cambridge University Press

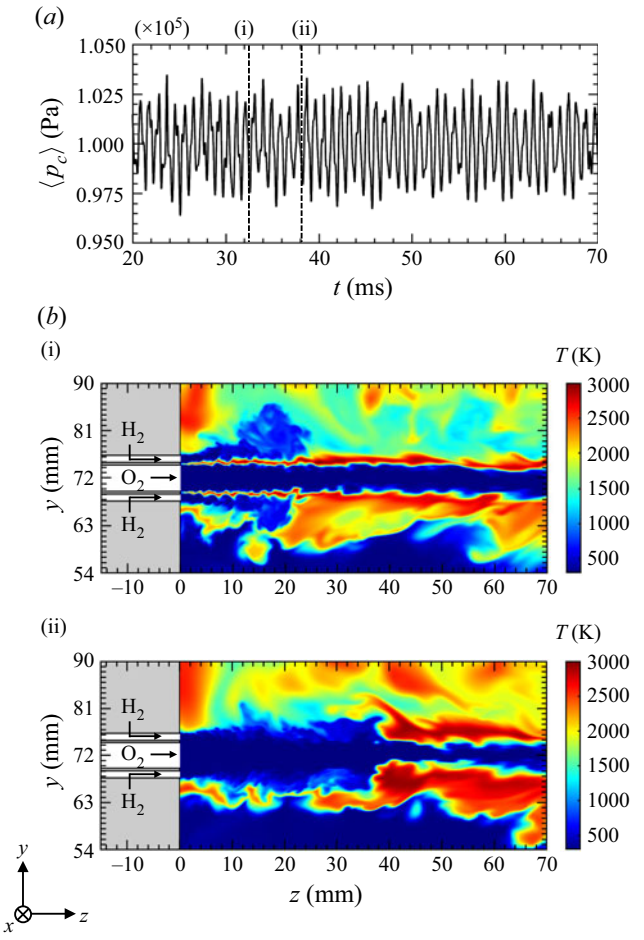

Figure 1. (*a*) Time variation in spatially averaged pressure fluctuations $\langle p_c \rangle$ during combustion instability in the ranges of $x = 0$ mm, $54\,\text{mm} \leq y \leq 90\,\text{mm}$ and $0\,\text{mm} < z \leq 70\,\text{mm}$. (*b*) Instantaneous temperature field T in the combustion chamber during high-frequency combustion instability; (*a* (i),*b* (i)) $t = 32.55$ ms and (*a* (ii),*b* (ii)) $t = 38.25$ ms.

Hashimoto *et al.* 2019) shedding from the injector rim (figure 1*b*). The location of the flame edge changes up to $z \approx 50$ mm when the flame edge is lifted from the injector rim, where z is the longitudinal direction of the combustor. The ignition of the unburnt H_2/O_2 mixture periodically arises shortly after the unburnt H_2/O_2 mixture that moves upward and touches high-temperature combustion products (Matsuyama *et al.* 2016; Shima *et al.* 2021). As a result of the periodic ignition, the attached flame forms near the injector rim. We focus on the region ($x = 0$ mm, $64\,\text{mm} \leq y \leq 80\,\text{mm}$ and $0\,\text{mm} < z \leq 70\,\text{mm}$, where x is the direction normal to the y direction) covering the flame dynamics during high-frequency combustion instability (see figure 1*b*).

2.1. *Rayleigh index ratio*

The Rayleigh index, which is derived from the acoustic energy equation, is widely used as an important indicator for extracting the driving region of combustion instability (Lieuwen 2012). Lieuwen (2012) explained that the molecular source term considering the changes

https://doi.org/10.1017/jfm.2023.52 Published online by Cambridge University Press

in the number of moles in the gas throughout chemical reactions works as one of the source terms in the acoustic energy equation under oxygen combustion. Aoki *et al.* (2017) showed that the energy budget of the acoustic production should be considered for the estimation of the Rayleigh index. On these bases, we propose a local Rayleigh index ratio considering the effects of heat release rate and molecular production as the source term in the acoustic energy equation. In this index, we define the source term Φ as (2.1).

$$\Phi = \frac{\gamma_0 - 1}{\gamma_0 p_0} p_1 q_1 + p_1 \left(\frac{\dot{n}}{n}\right)_1. \tag{2.1}$$

The first (second) term of the right-hand side of (2.1) corresponds to the heat release rate source term (molecular production source term)

$$R_{I,h} = \frac{1}{T_p} \int_{T_p} \left\{ \frac{\gamma_0 - 1}{\gamma_0 p_0} p_1 q_1 \right\} \mathrm{d}t. \tag{2.2}$$

$$R_{I,m} = \frac{1}{T_p} \int_{T_p} \left\{ p_1 \left(\frac{\dot{n}}{n}\right)_1 \right\} \mathrm{d}t. \tag{2.3}$$

$$\xi_R = \frac{R_{I,h} + R_{I,m}}{R_{I,h}}. \tag{2.4}$$

Here, $R_{I,h}(R_{I,m})$ is a local Rayleigh index based on the heat release rate source (molecular production source), ξ_R is a local Rayleigh index ratio, γ is the specific heat ratio, p is the pressure inside the combustor, q is the heat release rate, n is the mole concentration, $\dot{n} = \sum_{i=1}^{N_s} (\dot{w}_i / M_{w,i})$, where N_s is the total number of chemical species, $M_{w,i}$ is the molecular weight of species i and $\dot{w}_i$ is the mass-based production rate of species i by chemical reactions, and subscript 0 (1) represents a time-averaged (fluctuation) quantity. The physical meaning of ξ_R is that the mole production source does not affect the driving of combustion instability when ξ_R equals unity ($R_{I,m} = 0$). The mole production source acts as the amplification (attenuation) of combustion instability when ξ_R is larger (smaller) than unity. Note that T_p is set to 10 ms in this study so as to eliminate the dependence of T_p on the spatial distributions of $R_{I,h}$, $R_{I,m}$ and ξ_R.

2.2. *Acoustic energy flux-based spatial network*

Krishnan *et al.* (2019*b*) and Shima *et al.* (2021) studied the formation and collapse of the acoustic power source in the acoustic power network. In this study, we propose an acoustic energy flux-based spatial network as a new complex network. Let us assume that the total acoustic energy source produced at a local region $\Delta y \Delta z$ can be expressed as $\Phi \Delta y \Delta z$. Our network considers the energy flux I_{ij} at location $\boldsymbol{y}_j$ induced by the acoustic energy source $\Phi(\boldsymbol{y}_i)$ per unit time volume at another location $\boldsymbol{y}_i$ as follows:

$$I_{ij} = \frac{|\Phi(\boldsymbol{y}_i) \Delta y \Delta z|}{2\pi |\boldsymbol{y}_i - \boldsymbol{y}_j|}. \tag{2.5}$$

Here, $\Delta y(\Delta z)$ is the grid size in the $y(z)$ direction over a Cartesian domain and a grid corresponds to a node in the network. Equation (2.5) physically means that the energy flux ($= \Phi \Delta y \Delta z / r$) propagates to a location r away from $\Delta y \Delta z$ when the total acoustic energy spreads isotropically. On this basis, we define the weight of the link between nodes

https://doi.org/10.1017/jfm.2023.52 Published online by Cambridge University Press

as (2.6), where w_{ij} represents the mean energy flux between I_{ij} and I_{ji}

$$w_{ij} = \frac{1}{2}\left(I_{ij} + I_{ji}\right). \tag{2.6}$$

We construct three networks consisting of weighted adjacent matrices: $\boldsymbol{A}_{\pm}$, $\boldsymbol{A}_{+}$ and $\boldsymbol{A}_{-}$. All the nodes except for $i = j$ are connected in the first network. The nodes in the second network (third network) are connected when $\Phi(\boldsymbol{y}_i) > 0$ ($\Phi(\boldsymbol{y}_i) < 0$), corresponding to the amplification (attenuation) of acoustic energy. We estimate the node strengths $s_{\pm,i}$, $s_{+,i}$, and $s_{-,i}$ as follows:

$$A_{\pm,ij} = \begin{cases} w_{ij}, & \text{if } i \neq j, \\ 0, & \text{otherwise.} \end{cases} \tag{2.7}$$

$$A_{+,ij} = \begin{cases} w_{ij}, & \text{if } \Phi(\boldsymbol{y}_i) > 0 \text{ and } \Phi(\boldsymbol{y}_j) > 0 \ (i \neq j), \\ 0, & \text{otherwise.} \end{cases} \tag{2.8}$$

$$A_{-,ij} = \begin{cases} w_{ij}, & \text{if } \Phi(\boldsymbol{y}_i) < 0 \text{ and } \Phi(\boldsymbol{y}_j) < 0 \ (i \neq j), \\ 0, & \text{otherwise.} \end{cases} \tag{2.9}$$

$$s_i = \sum_{j=1}^{N} A_{ji}. \tag{2.10}$$

Here, N is the number of nodes and $N = 19\,360$ in this study.

2.3. *Community detection*

Murayama *et al.* (2018) have recently extracted the community in the turbulent network during intermediate-frequency combustion instability in a swirl-stabilized combustor by the Louvain method based on modularity optimization (Blondel *et al.* 2008; Jeub *et al.* 2011–2019). In this study, we adopt the Louvain method for the acoustic energy flux-based spatial network. Newman (2004) proposed the modularity Q as an important index of the division accuracy of a community. We extract the community by computing the gain ΔQ obtained by moving an isolated node i into community $C_{a,k}$ as

$$Q = \frac{1}{2m}\sum_{i=1}^{N}\sum_{j=1}^{N}\left(A_{ij} - \frac{s_i s_j}{2m}\right)\delta(c_{a,i}, c_{a,j}). \tag{2.11}$$

$$\Delta Q = \left[\frac{\Sigma_{in} + 2s_{i,in}}{2m} - \left(\frac{\Sigma_{tot} + s_i}{2m}\right)^2\right] - \left[\frac{\Sigma_{in}}{2m} - \left(\frac{\Sigma_{tot}}{2m}\right)^2 - \left(\frac{s_i}{2m}\right)^2\right]. \tag{2.12}$$

Here, m is the sum of the weights of all links in the network ($= \frac{1}{2}\sum_{i=1}^{N} s_i$), Σ_{in} is the sum of the weights of the links inside $C_{a,k}$, Σ_{tot} is the sum of the weights of the links incident to the nodes in $C_{a,k}$, $s_{i,in}$ is the sum of the weights of the links from node i to other nodes in $C_{a,k}$ and $\delta(c_{a,i}, c_{a,j})$ is the Kronecker delta. A suitable total number of communities is determined so as to maximize the modularity (Q becomes maximum when the sign of ΔQ changes from positive to negative).

Guimerà & Amaral (2005) proposed the P–Z map as a useful tool for understanding the structure of complex networks. Meena & Taira (2021) studied the spatio-temporal

https://doi.org/10.1017/jfm.2023.52 Published online by Cambridge University Press

dynamics of the vortical structure by examining the P–Z map of the turbulence network. In this study, we adopt the P–Z map for the acoustic energy flux-based spatial network. We first define $s_{i,k}$ at node i as the sum of the weights of the links adjacent to the nodes in community $C_{a,k}$

$$s_{i,k} = \sum_{j=1, c_j \in \hat{C}_{a,k}}^{N} A_{ji}. \tag{2.13}$$

Here, $c_{a,i}$ is the community to which node i belongs and $\hat{C}_{a,k}$ is the set of communities k. The participation coefficient P_i and the within-community degree z-score Z_i are respectively given by (2.14) and (2.15), where $\langle s_{i,c_{a,i}} \rangle$ ($\sigma_{s_{i,c_{a,i}}}$) is the mean value (standard deviation) of $s_{i,c_{a,i}}$

$$P_i = 1 - \sum_{k=1}^{N_c} \left(\frac{s_{i,k}}{s_i} \right)^2. \tag{2.14}$$

$$Z_i = \frac{s_{i,c_{a,i}} - \langle s_{i,c_{a,i}} \rangle}{\sigma_{s_{i,c_{a,i}}}}. \tag{2.15}$$

Here, N_c is the total number of communities and Z_i represents the degree of connection between node i and other nodes in the same community. When Z_i takes a high value, node i is strongly connected with other nodes and becomes the hub in the community. As P_i takes a high value, a node is homogeneously connected with all the nodes in the community. Note that $0 \leq P_i \leq 1$.

2.4. *Spectral clustering*

Spectral clustering (Newman 2006; Von Luxburg 2007) is a useful unsupervised machine learning method and is performed by applying the k-means method to the eigenvectors of the Laplacian matrix in complex networks. In this study, we first construct a three-dimensional plane consisting of the pressure and flow velocity of the hydrogen jet at the injector exit, and the temperature near the injector rim. The latent space with K clusters is obtained by applying the spectral-clustering method and the Gaussian kernel transformation to the three-dimensional plane. We finally obtain a transition network of clusters from the latent space. The value of K is set to 12 in this study (see Appendix A).

3. Results and discussion

Figure 2 shows the spatial distributions of $R_{I,h}$, $R_{I,m}$ and ξ_R during high-frequency combustion instability at 30 ms $\leq t \leq$ 40 ms. The value of $R_{I,h}$ is larger than zero along the shear layer region between the hydrogen and oxygen jets, revealing the driving region of combustion instability as a result of the production of acoustic energy due to the strong mutual coupling between the pressure and heat release rate fluctuations. In contrast, $R_{I,m}$ is less than zero along the shear layer region, indicating that the mutual coupling between the molecular production and pressure fluctuations attenuates combustion instability. The value of ξ_R is approximately 0.9, which shows that the molecular production term contributes to the decrease in acoustic energy that originates from the heat release rate term and ξ_R also decreases in the radial direction. This means that the attenuation of the acoustic energy due to molecular production is greater in the hydrogen jet region than

https://doi.org/10.1017/jfm.2023.52 Published online by Cambridge University Press

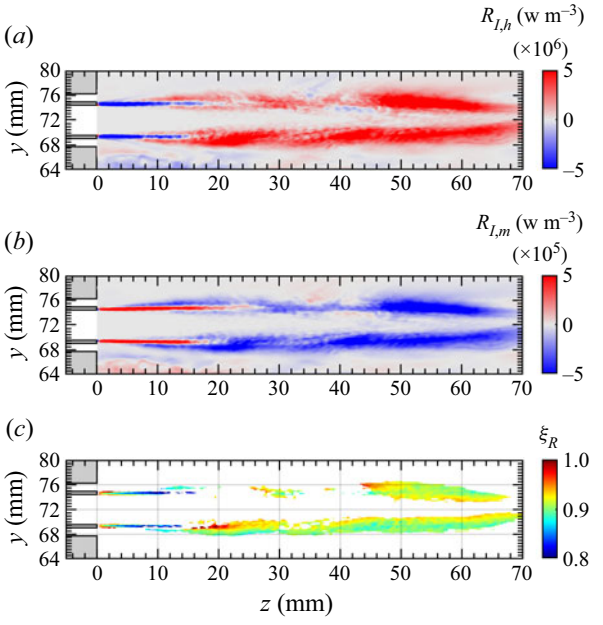

Figure 2. Spatial distributions of local Rayleigh indices (*a*) $R_{I,h}$ based on the heat release rate term, (*b*) $R_{I,m}$ based on the molecular production term and (*c*) local Rayleigh index ratio ξ_R during high-frequency combustion instability at 30 ms $\leq t \leq$ 40 ms.

in the oxygen jet region. The damping effect on high-frequency combustion instability (approximately 10 % with respect to the heat release rate term) is non-negligible for inferring the driving region of high-frequency combustion instability, which supports the importance of the molecular production term explained by Lieuwen (2012). These results demonstrate that the local Rayleigh index ratio consisting of the heat release rate and molecular production terms is significant for inferring the driving region of high-frequency combustion instability in a model rocket combustor with a hydrogen/oxygen injector.

Figure 3 shows the time variation in the spatially averaged pressure fluctuations $\langle p_c \rangle$, heat release rate fluctuations $\langle q \rangle$ and node strengths $\langle s_{\pm,i} \rangle$, $\langle s_{+,i} \rangle$ and $\langle s_{-,i} \rangle$ during high-frequency combustion instability in the ranges of $x = 0$ mm, 64 mm $\leq y \leq$ 80 mm and 0 mm $< z \leq$ 70 mm. We observe that $\langle p_c \rangle$ fluctuates periodically, whereas $\langle q \rangle$ exhibits intermittent fluctuations responding to the attachment and detachment of the flame edge from the injector rim. Node strength $\langle s_{\pm,i} \rangle$ exhibits periodic fluctuations with half the period of $\langle p_c \rangle$ and increases when $\langle p_c \rangle$ takes the local value, and $\langle s_{\pm,i} \rangle$ markedly increases when $\langle q \rangle$ changes owing to the detachment of the flame edge. An important point to emphasize here is that $\langle s_{+,i} \rangle$ is considerably larger than $\langle s_{-,i} \rangle$ when $\langle p_c \rangle$ takes the local minimum owing to the detachment of the flame edge. These results show that the acoustic energy production is promoted when the flame edge is detached from the injector rim, resulting in the retention of combustion instability. The spatial distributions of $s_{\pm,i}$ are shown in figure 4, together with the probability distributions of the node strengths $P_{s_\pm}$, P_{s_+} and P_{s_-}. The nodes with high strength are distributed along the shear layer region at $t = 32.55$ ms. The coefficients of determination R^2 for $P_{s_\pm}$, P_{s_+} and P_{s_-} exceed 0.9. The scale-free nature appears for all the probability distributions of the node strength. The scaling exponents γ_s for $P_{s_\pm}$, P_{s_+} and P_{s_-} are 2.6, 2.8 and 2.4, respectively, which show that the existing probabilities of the hub are almost

https://doi.org/10.1017/jfm.2023.52 Published online by Cambridge University Press

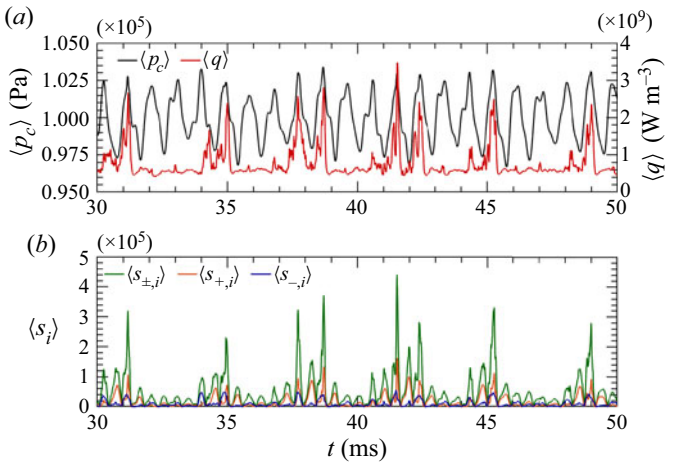

Figure 3. (*a*) Time variation in the spatially averaged pressure fluctuations $\langle p_c \rangle$ and heat release rate fluctuations $\langle q \rangle$, and (*b*) time variation in the average node strengths in the acoustic energy flux-based spatial network during high-frequency combustion instability.

the same. This means that the acoustic production and damping sources are equally formed when the flame edge is attached to the injector rim. In contrast, the scale-free nature of $P_{s_\pm}$, P_{s_+} and P_{s_-} collapses at $t = 38.25$ ms. An important observation is the expansion of the formation region of the nodes with high strength, including the emergence of a large-scale primary hub. This means that the formation of a large-scale acoustic energy source drives combustion instability when the flame edge is detached. The results shown in figures 3 and 4 indicate that the acoustic energy flux-based spatial network proposed in this study enables the production of the acoustic energy source with accompanying intermittent heat release rate fluctuations to be captured. In this paper, we have presented the spatial distributions of the local Rayleigh indices $R_{I,h}$, $R_{I,m}$ and ξ_R during 10 cycles of high-frequency combustion instability to infer the driving region of high-frequency combustion instability. The acoustic energy flux-based spatial network, which enables us to instantaneously extract the acoustic energy source, is superior to the local Rayleigh indices, in the sense that the acoustic energy flux-based spatial network can capture the subtle changes in the acoustic energy source in response to the flame behaviour with fast switching between detachment and attachment on the injector rim. Note that the quantification of the network structure using three node strengths, $s_\pm$, s_+ and s_-, which identify both the amplification and attenuation regions of acoustic power, has not been conducted in previous studies on combustion instability.

Figure 5 shows the community and the *P*–*Z* map at the time of attachment of the flame edge to the injector rim. Here, $\langle P_i \rangle$ (Z_{max}) is the mean (maximum) of P_i (Z_i) in community $C_{a,k}$. The black markers correspond to the centre of $C_{a,k}$ and the plot size represents the sum of the node strengths in the community. The width of the grey line represents the degree of connection between the communities. The small communities are formed along the shear layer. The connection between them is strong near the injector rim and weakens downstream. Some communities take high (low) $\langle P_i \rangle$ and Z_{max} values near the injector rim (downstream). This means that the communities possess a hub near the injector rim, whereas it vanishes downstream with the formation of isolated communities. These results show that the acoustic energy source induced near the injector rim collapses downstream when the flame edge is attached to the injector rim. The community and

https://doi.org/10.1017/jfm.2023.52 Published online by Cambridge University Press

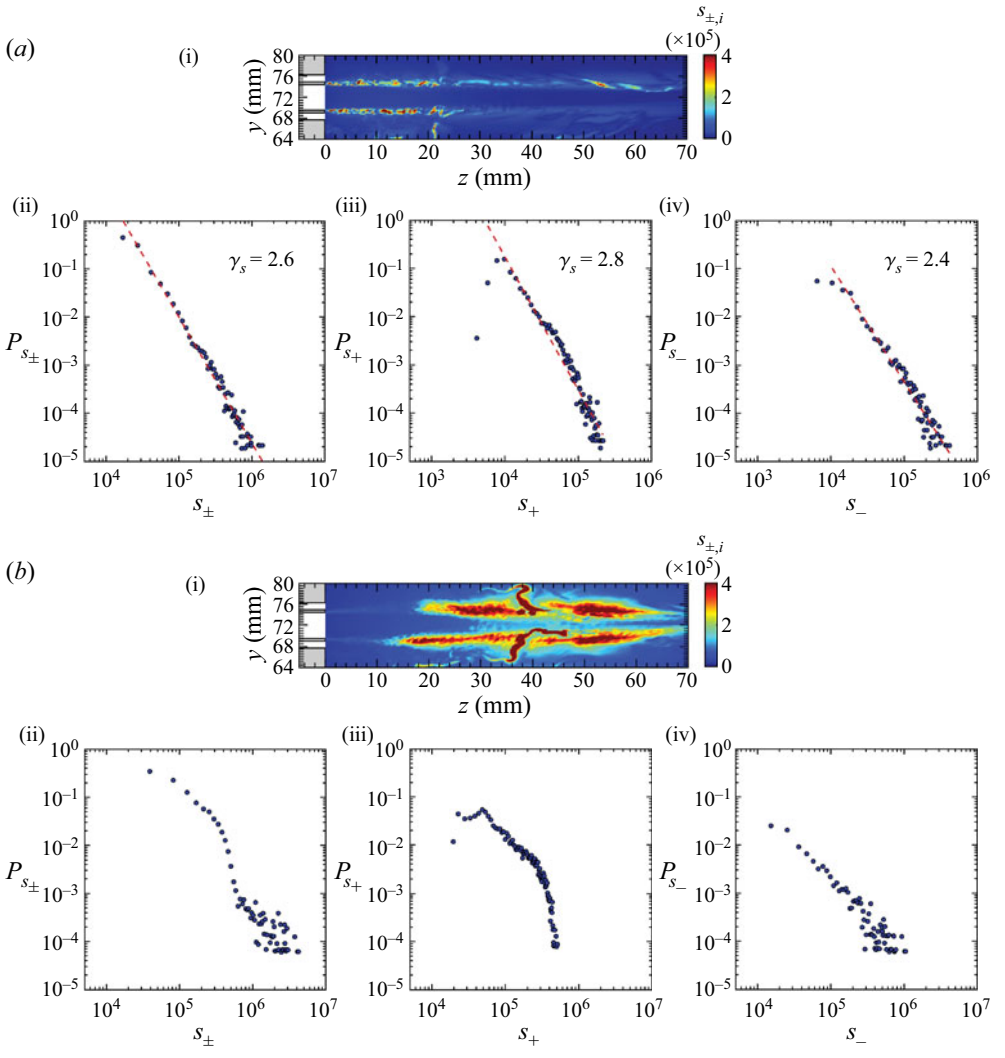

Figure 4. (*a* (i),*b* (i)) Spatial distributions of the node strengths $s_{\pm,i}$ and (*a* (ii–iv),*b* (ii–iv)) probability distributions of the node strengths $P_{s_\pm}$, P_{s_+} and P_{s_-} in the acoustic energy flux-based spatial network during high-frequency combustion instability; (*a*) $t = 32.55$ ms and (*b*) $t = 38.25$ ms.

the *P*–*Z* map at the time of detachment of the flame edge from the injector rim is shown in figure 6. Communities appear downstream at $t = 37.55$ ms. Large communities with strong connection are formed along the shear layer when $\langle p_c \rangle$ and $\langle q \rangle$ take a local maximum at $t = 37.75$ ms. The formation of the large communities is attributed to the reignition upstream after the flame edge moves downstream. The connection between the communities weakens at $t = 37.95$ ms, whereas it strengthens again when $\langle p_c \rangle$ and $\langle q \rangle$ take a local minimum at $t = 38.25$ ms. Communities with high Z_{max} are formed at $t = 37.75$ ms compared with those at $t = 38.25$ ms, which indicates the appearance of a dominant hub in the communities due to the ignition of the H_2/O_2 flame when the pressure and heat release rate fluctuations take a local maximum. In contrast, communities with high $\langle P_i \rangle$ are formed at $t = 38.25$ ms compared with those at $t = 37.75$ ms. This indicates that the movement of the flame edge downstream causes the connection of the communities to strengthen

https://doi.org/10.1017/jfm.2023.52 Published online by Cambridge University Press

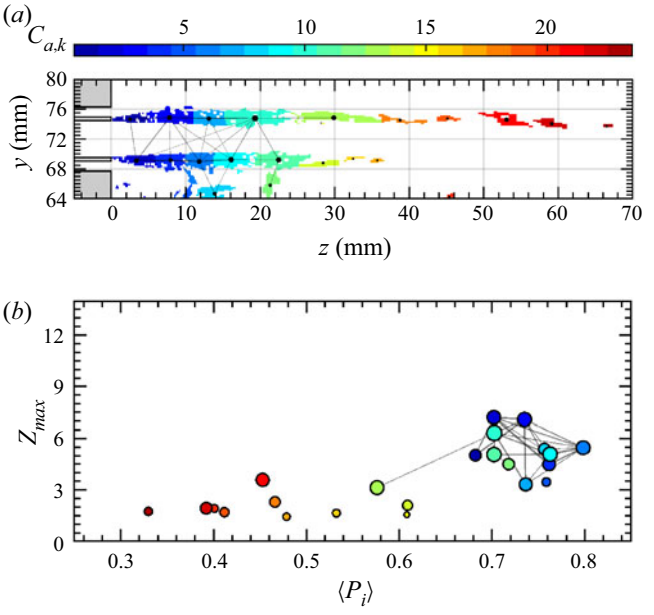

Figure 5. (*a*) Community and (*b*) *P*–*Z* map at the time of attachment of the flame edge to the injector rim during high-frequency combustion instability. Here, $t = 32.55$ ms.

when the pressure and heat release rate fluctuations take a local minimum. High-frequency combustion instability in this study is maintained accompanying the changes in these community structures. The Indian Institute of Technology Madras group and other groups have conducted detailed experimental studies on the emergence and collapse of the clusters in the spatial network during combustion instability in a bluff-body-stabilized combustor (Krishnan *et al.* 2019*a*,*b*) and a model rocket combustor with multiple elements (Kasthuri *et al.* 2022). One of the authors (Murayama *et al.* 2018) has also conducted an experimental study on the formation of a primary hub in a turbulent network during intermediate-frequency combustion instability in a swirl-stabilized turbulent combustor. The community detection using the acoustic energy flux-based spatial network is expected to be helpful for understanding the spatio-temporal characteristics of the clusters and their connections during combustion instability in various combustors, although the flame dynamics depends on the chemical and flow characteristic time scales and configuration of combustors.

Figure 7 shows the time variation in the temperature T near the injector exit. Note that the temperature at $z = 0.46$ mm is extracted as a representative location. An abrupt increase in T is intermittently observed in the range of 68 mm $\leq y \leq$ 76 mm, showing the inflow of combustion products into the H_2 jet near the injector rim. This is strongly associated with the reignition of the H_2/O_2 mixture. Matsuyama *et al.* (2016) reported that the decrease in flow velocity at the exit of a H_2 injector generates the inflow of combustion products into the injector. Shima *et al.* (2021) have recently clarified that the pressure fluctuations inside a combustor significantly affect the flow velocity fluctuations in the H_2 injector. On the basis of these findings, we examine the structure of the spectral-clustering-based transition network constructed from the pressure p_e at the exit of the H_2 injector, the flow velocity w_e of the H_2 jet at the exit of the injector and the temperature T_r near the injector rim.

https://doi.org/10.1017/jfm.2023.52 Published online by Cambridge University Press

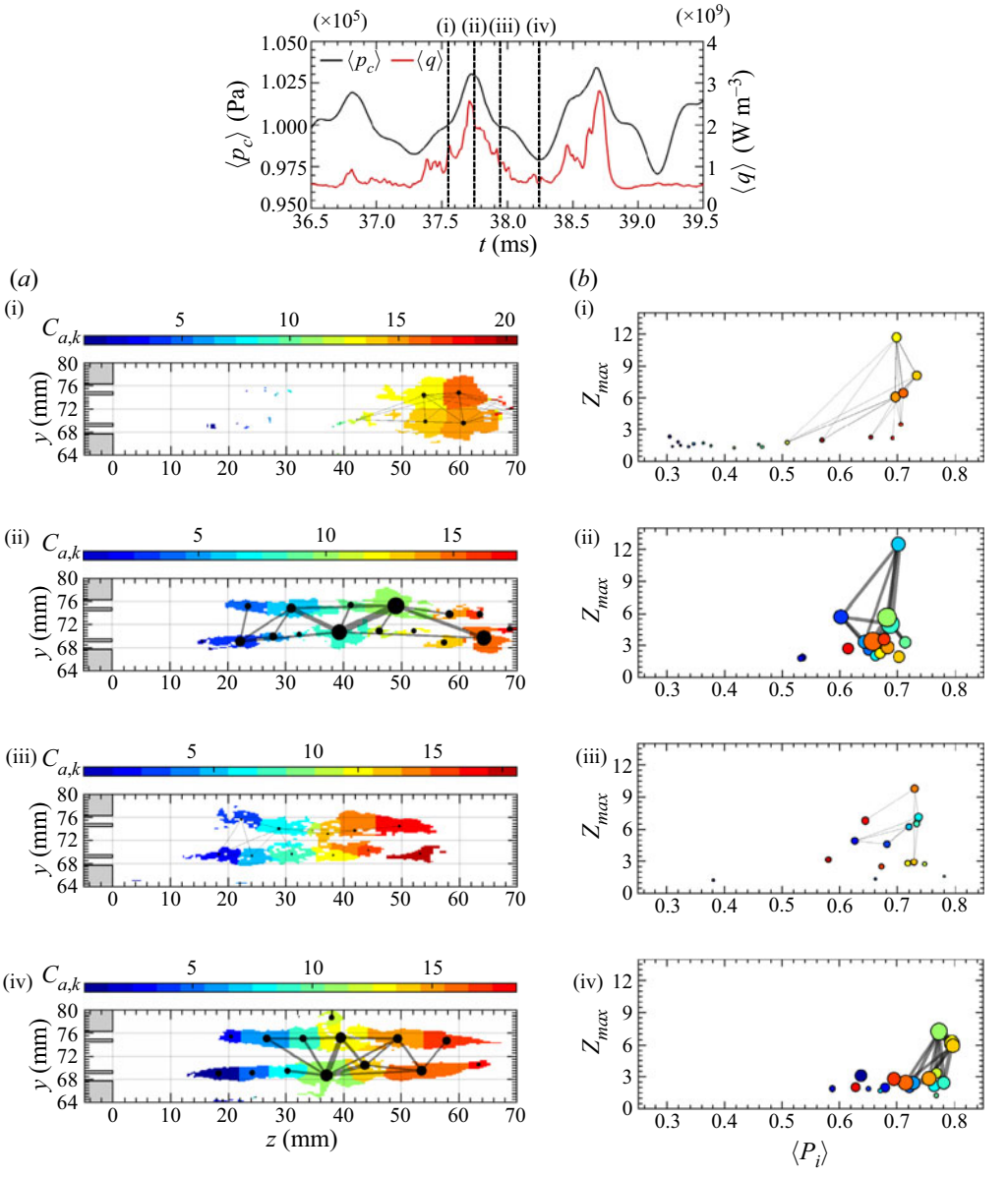

Figure 6. Time variations in (*a*) community and (*b*) *P*–*Z* map at the time of detachment of the flame edge from the injector rim during high-frequency combustion instability; (*a* (i),*b* (i)) $t = 37.55$ ms, (*a* (ii),*b* (ii)) $t = 37.75$ ms, (*a* (iii),*b* (iii)) $t = 37.95$ ms and (*a* (iv),*b* (iv)) $t = 38.25$ ms.

Figure 8 shows the latent space consisting of $\langle w_e \rangle$, $\langle p_e \rangle$ and $\langle T_r \rangle$ and the centroid of cluster $C_{t,k}$ in the latent space during high-frequency combustion instability, together with the transition network between the clusters. Note that, in this study, we define $\langle w_e \rangle$, $\langle p_e \rangle$ and $\langle T_r \rangle$ as the spatially averaged values of w_e, p_e and T_r at (y_1, z_1) and (y_2, z_2), respectively, where $(y_1, z_1) = (68.4\,\text{mm}, 0.46\,\text{mm})$ and $(y_2, z_2) = (75.6\,\text{mm}, 0.46\,\text{mm})$ for $\langle w_e \rangle$ and $\langle p_e \rangle$, and $(y_1, z_1) = (69.3\,\text{mm}, 0.46\,\text{mm})$ and $(y_2, z_2) = (74.7\,\text{mm}, 0.46\,\text{mm})$ for $\langle T_r \rangle$. Here, $\langle w_e \rangle_c$, $\langle p_e \rangle_c$ and $\langle T_r \rangle_c$ correspond to the centroid of the cluster, and

https://doi.org/10.1017/jfm.2023.52 Published online by Cambridge University Press

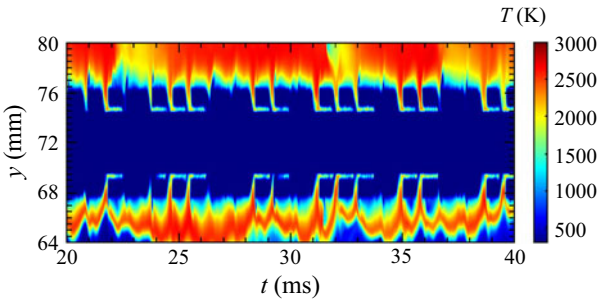

Figure 7. Time variation in the temperature T near the injector exit during high-frequency combustion instability. Here, $z = 0.46$ mm.

the width of the grey line in the network represents the transition probability between the clusters. The network exhibits two predominant orbits: (I) cluster $1 \to 2 \to 3 \to 4 \to 5 \to 6$ and (II) cluster $6 \to 7 \to 8 \to 9 \to 10 \to 11 \to 12$. They are connected to each other at cluster 6. The centre node of the cluster of the temperature $\langle T_r \rangle_c$ remains unchanged in orbit I, whereas it changes in orbit II. This indicates that cluster 6 corresponds to the critical state of the detached flame edge from the injector rim. We observe that $\langle T_r \rangle_c$ takes a maximum value at cluster 8. On the basis of the finding shown in figure 7, cluster 8 corresponds to the inflow of combustion products into the H_2 jet near the injector rim and the subsequent reignition of the H_2/O_2 mixture. An important point is that the trajectory of the cluster bifurcates at cluster 6 and $\langle w_e \rangle_c$ takes a positive (negative) value at cluster 1 (7). This means that the subtle change in the flow velocity of the H_2 jet at the injector exit has a significant impact on the triggering of the bifurcation into the attachment and detachment of the flame edge, and the onset of the intermittent heat release rate fluctuations during high-frequency combustion instability. Note that cluster 6 is the bifurcation point for the sudden switching between the attached and lifted flame edges, but the dynamic behaviour of the pressure does not notably change before and after the bifurcation. These results demonstrate that the spectral-clustering-based transition network is useful for understanding the physical mechanism of high-frequency combustion instability in a model rocket combustor with a hydrogen/oxygen injector.

4. Summary

We have studied the spatio-temporal dynamics of high-frequency combustion instability in a cylindrical combustor with an off-centre-installed coaxial injector related to a H_2/O_2 rocket combustor from the viewpoint of complex networks and machine learning, focusing mainly on the production of the acoustic energy source. The molecular production induced by combustion reaction affects the attenuation of combustion instability, which is shown by a local Rayleigh index ratio considering both the heat release rate and molecular production terms. The pressure inside the combustor oscillates periodically, whereas the heat release rate exhibits intermittent fluctuations responding to the attachment and detachment of the flame edge from the injector rim. The acoustic energy flux-based spatial network we proposed in this study enables the appearance of the acoustic energy source with accompanying intermittent heat release rate fluctuations to be captured. When the flame edge is attached to the injector rim, nodes with high strength are formed in the upstream region of the shear layer between the oxygen and hydrogen jets, exhibiting a scale-free nature in the strength distribution. The acoustic energy source collapses by the formation of small communities with weak connection. In contrast, when the flame

https://doi.org/10.1017/jfm.2023.52 Published online by Cambridge University Press

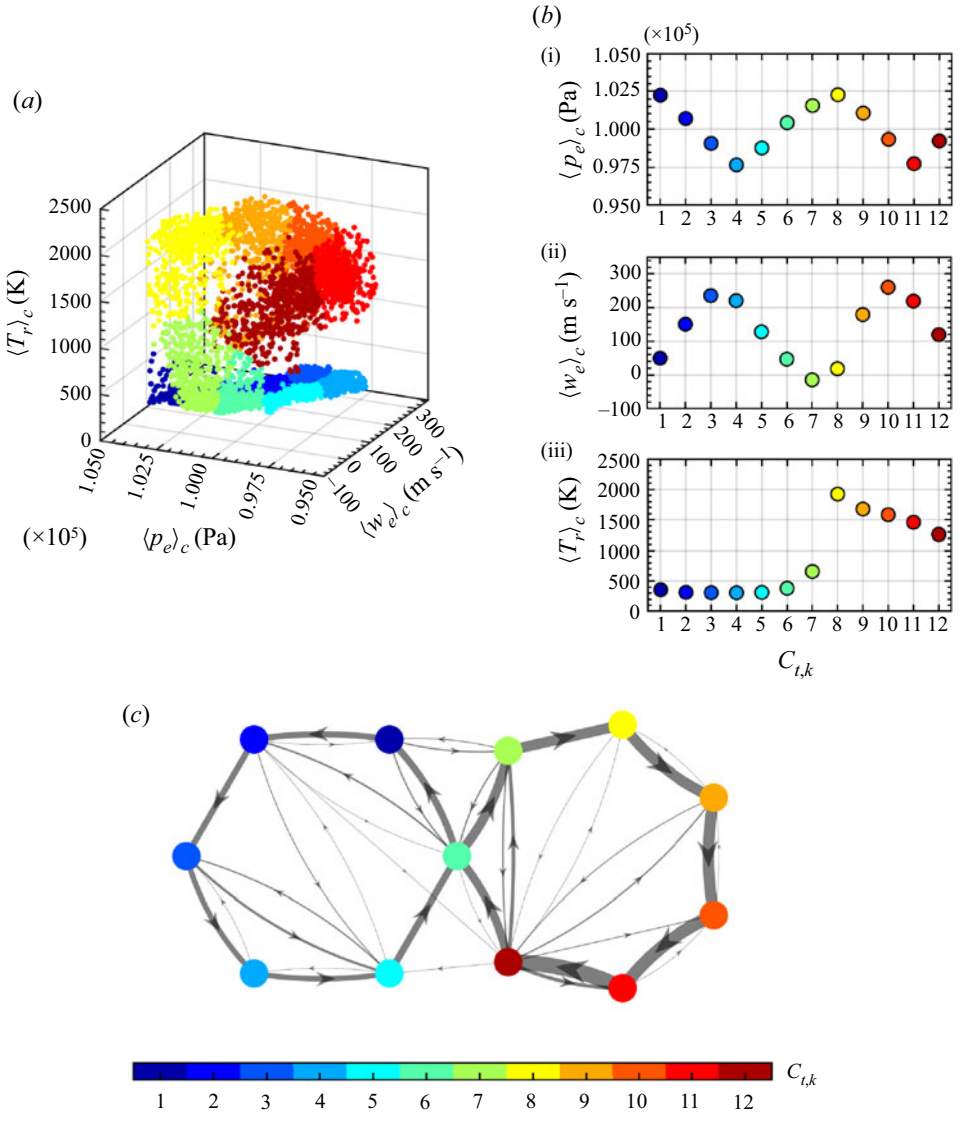

Figure 8. (*a*) Latent space consisting of the spatially averaged pressure $\langle p_e \rangle$ at the H_2 injector exit, the flow velocity $\langle w_e \rangle$ of the H_2 jet at the injector exit and the temperature $\langle T_r \rangle$ near the injector rim during high-frequency combustion instability, (*b*) centroid of cluster $C_{t,k}$ in the latent space and (*c*) spectral-clustering-based transition network.

edge is detached from the injector rim, nodes with high strength are widely formed in the downstream region of the shear layer, revealing the loss of the scale-free nature. The formation of large communities with strong connection has a significant impact on driving combustion instability. The switching between the attachment and detachment of the flame edge during combustion instability can be explained by the spectral-clustering-based transition network constructed from the pressure and flow velocity of the hydrogen jet at the injector exit, and the temperature near the injector rim. The two presented analyses: (i) community detection using the acoustic energy flux-based spatial network and (ii) spectral

https://doi.org/10.1017/jfm.2023.52 Published online by Cambridge University Press

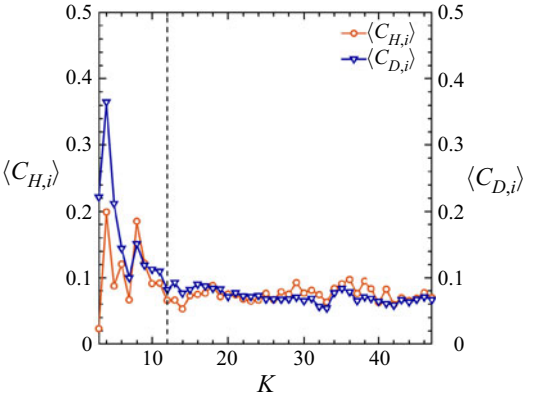

Figure 9. Variations in the average cluster coefficients $\langle C_{H,i}\rangle$ and $\langle C_{D,i}\rangle$ as a function of the class number K during high-frequency combustion instability.

clustering as a form of unsupervised machine learning, are useful for understanding the complex spatio-temporal dynamics of combustion instability.

Declaration of interests. The authors report no conflict of interest.

Author ORCIDs.
Kazuki Kawano https://orcid.org/0000-0003-0161-0305;
Hiroshi Gotoda https://orcid.org/0000-0001-6402-8510;
Yusuke Nabae https://orcid.org/0000-0001-7560-5053;
Yuya Ohmichi https://orcid.org/0000-0002-0812-1267;
Shingo Matsuyama https://orcid.org/0000-0002-1543-1925.

Appendix A. Class number in the cluster-based transition network

We determine a suitable class number K in the cluster-based transition network by estimating two cluster coefficients. The weighted cluster coefficients $C_{H,i}$ (Holme *et al.* 2007) and $C_{D,i}$ (Fagiolo 2007) are defined as (A1) and (A2), respectively,

$$C_{H,i} = \frac{\displaystyle\sum_{j=1}^{N_t}\sum_{k=1}^{N_t} A^*_{t,ij}A^*_{t,jk}A^*_{t,ki}}{\max(\boldsymbol{A}^*_t)\displaystyle\sum_{j=1}^{N_t}\sum_{k=1}^{N_t} A^*_{t,ij}A^*_{t,ki}}, \tag{A1}$$

$$C_{D,i} = \frac{\displaystyle\sum_{j=1}^{N_t}\sum_{k=1}^{N_t}\left(A_{t,ij}+A_{t,ji}\right)\left(A_{t,jk}+A_{t,kj}\right)\left(A_{t,ki}+A_{t,ik}\right)}{2\left[\displaystyle\sum_{j=1}^{N_t}\left(A_{t,ij}+A_{t,ji}\right)\left\{\sum_{j=1}^{N_t}\left(A_{t,ij}+A_{t,ji}\right)-1\right\}-2\sum_{j=1}^{N_t}\left(A_{t,ij}A_{t,ji}\right)\right]}. \tag{A2}$$

Here, $\boldsymbol{A_t}$ is the directed-adjacent matrix of the transition network, and $\boldsymbol{A^*_t}(=\frac{1}{2}(\boldsymbol{A_t}+\boldsymbol{A_t^T}))$ is the undirected-adjacent matrix. The value of N_t is set to 5000 in this study.

https://doi.org/10.1017/jfm.2023.52 Published online by Cambridge University Press

Figure 9 shows the variations in the average cluster coefficients $\langle C_{H,i} \rangle$ and $\langle C_{D,i} \rangle$ as a function of K during high-frequency combustion instability. The value of $\langle C_{H,i} \rangle$ and $\langle C_{D,i} \rangle$ are nearly unchanged when K exceeds approximately 12. The latent space obtained by the spectral-clustering method can be appropriately divided into clusters in the transition network at $K \geq 12$. On this basis, we set K to 12 in this study.

References

Aoki, C., Gotoda, H., Yoshida, S. & Tachibana, S. 2020 Dynamic behavior of intermittent combustion oscillations in a model rocket engine combustor. *J. Appl. Phys.* **127** (22), 224903.

Aoki, K., Shimura, M., Naka, Y. & Tanahashi, M. 2017 Disturbance energy budget of turbulent swirling premixed flame in a cuboid combustor. *Proc. Combust. Inst.* **36** (3), 3809–3816.

Armbruster, W., Hardi, J.S. & Oschwald, M. 2021 Flame-acoustic response measurements in a high-pressure, 42-injector, cryogenic rocket thrust chamber. *Proc. Combust. Inst.* **38** (4), 5963–5970.

Barabási, A.-L. 2016 *Network Science*. Cambridge University Press.

Bishop, C.M. 2006 *Pattern Recognition and Machine Learning*. Springer.

Blondel, V.D., Guillaume, J.-L., Lambiotte, R. & Lefebvre, E. 2008 Fast unfolding of communities in large networks. *J. Stat. Mech.* **2008** (10), P10008.

Brear, M.J., Nicoud, F., Talei, M., Giauque, A. & Hawkes, E.R. 2012 Disturbance energy transport and sound production in gaseous combustion. *J. Fluid Mech.* **707**, 53–73.

Fagiolo, G. 2007 Clustering in complex directed networks. *Phys. Rev.* E **76** (2), 026107.

Godavarthi, V., Pawar, S.A., Unni, V.R., Sujith, R.I., Marwan, N. & Kurths, J. 2018 Coupled interaction between unsteady flame dynamics and acoustic field in a turbulent combustor. *Chaos* **28** (11), 113111.

Gröning, S., Hardi, J.S., Suslov, D. & Oschwald, M. 2016 Injector-driven combustion instabilities in a hydrogen/oxygen rocket combustor. *J. Propul. Power* **32** (3), 560–573.

Guan, Y., Li, L.K.B., Ahn, B. & Kim, K.T. 2019 Chaos, synchronization, and desynchronization in a liquid-fueled diffusion-flame combustor with an intrinsic hydrodynamic mode. *Chaos* **29** (5), 053124.

Guan, Y., Moon, K., Kim, K.T. & Li, L.K.B. 2022 Synchronization and chimeras in a network of four ring-coupled thermoacoustic oscillators. *J. Fluid Mech.* **938**, A5.

Guimerà, R. & Amaral, L.A.N. 2005 Functional cartography of complex metabolic networks. *Nature* **433**, 895–900.

Hachijo, T., Masuda, S., Kurosaka, T. & Gotoda, H. 2019 Early detection of thermoacoustic combustion oscillations using a methodology combining statistical complexity and machine learning. *Chaos* **29** (10), 103123.

Harvazinski, M.E., Huang, C., Sankaran, V., Feldman, T.W., Anderson, W.E., Merkle, C.L. & Talley, D.G. 2015 Coupling between hydrodynamics, acoustics, and heat release in a self-excited unstable combustor. *Phys. Fluids* **27** (4), 045102.

Hashimoto, T., Shibuya, H., Gotoda, H., Ohmichi, Y. & Matsuyama, S. 2019 Spatiotemporal dynamics and early detection of thermoacoustic combustion instability in a model rocket combustor. *Phys. Rev.* E **99** (3), 032208.

Holme, P., Min Park, S., Kim, B.J. & Edling, C.R. 2007 Korean university life in a network perspective: dynamics of a large affiliation network. *Physica* A **373**, 821–830.

Huang, Y. & Yang, V. 2009 Dynamics and stability of lean-premixed swirl-stabilized combustion. *Prog. Energy Combust. Sci.* **35** (4), 293–364.

Iacobello, G., Ridolfi, L. & Scarsoglio, S. 2021 A review on turbulent and vortical flow analyses via complex networks. *Physica* A **563**, 125476.

Jeub, L.G.S., Bazzi, M., Jutla, I.S. & Mucha, P.J. 2011–2019 A generalized Louvain method for community detection implemented in MATLAB. http://netwiki.amath.unc.edu/GenLouvain.

Juniper, M.P. & Sujith, R.I. 2018 Sensitivity and nonlinearity of thermoacoustic oscillations. *Annu. Rev. Fluid Mech.* **50**, 661–689.

Kasthuri, P., Krishnan, A., Gejji, R., Anderson, W., Marwan, N., Kurths, J. & Sujith, R.I. 2022 Investigation into the coherence of flame intensity oscillations in a model multi-element rocket combustor using complex networks. *Phys. Fluids* **34** (3), 034107.

Kobayashi, T., Murayama, S., Hachijo, T. & Gotoda, H. 2019 Early detection of thermoacoustic combustion instability using a methodology combining complex networks and machine learning. *Phys. Rev. Appl.* **11** (6), 064034.

https://doi.org/10.1017/jfm.2023.52 Published online by Cambridge University Press

KOIZUMI, H., TSUTSUMI, S., OMATA, N. & SHIMIZU, T. 2020 Thermoacoustic coupling mechanism of combustion instability in a continuously variable resonance combustor. *AIAA Paper* 2020-1071.

KRISHNAN, A., MANIKANDAN, R., MIDHUN, P.R., REEJA, K.V., UNNI, V.R., SUJITH, R.I., MARWAN, N. & KURTHS, J. 2019*a* Mitigation of oscillatory instability in turbulent reactive flows: a novel approach using complex networks. *Europhys. Lett.* **128** (1), 14003.

KRISHNAN, A., SUJITH, R.I., MARWAN, N. & KURTHS, J. 2019*b* On the emergence of large clusters of acoustic power sources at the onset of thermoacoustic instability in a turbulent combustor. *J. Fluid Mech.* **874**, 455–482.

KRISHNAN, A., SUJITH, R.I., MARWAN, N. & KURTHS, J. 2021 Suppression of thermoacoustic instability by targeting the hubs of the turbulent networks in a bluff body stabilized combustor. *J. Fluid Mech.* **916**, A20.

LACASA, L., LUQUE, B., BALLESTEROS, F., LUQUE, J. & NUÑO, J.C. 2008 From time series to complex networks: the visibility graph. *Proc. Natl Acad. Sci. USA* **105** (13), 4972–4975.

LACASA, L. & TORAL, R. 2010 Description of stochastic and chaotic series using visibility graphs. *Phys. Rev.* E **82** (3), 036120.

LIEUWEN, T.C. 2012 *Unsteady Combustor Physics*. Cambridge University Press.

LIEUWEN, T.C. & YANG, V. 2005 *Combustion Instabilities in Gas Turbine Engines: Operational Experience, Fundamental Mechanisms, and Modeling*. American Institute of Aeronautics and Astronautics.

LLOYD, S. 1982 Least squares quantization in PCM. *IEEE Trans. Inf. Theory* **28** (2), 129–137.

MARTIN, J., ARMBRUSTER, W., HARDI, J.S., SUSLOV, D. & OSCHWALD, M. 2021 Experimental investigation of self-excited combustion instabilities in a LOX/LNG rocket combustor. *J. Propul. Power* **37** (6), 944–951.

MARWAN, N., ROMANO, M.C., THIEL, M. & KURTHS, J. 2007 Recurrence plots for the analysis of complex systems. *Phys. Rep.* **438** (5–6), 237–329.

MATSUYAMA, S., HORI, D., SHIMIZU, T., TACHIBANA, S., YOSHIDA, S. & MIZOBUCHI, Y. 2016 Large-eddy simulation of high-frequency combustion instability in a single-element atmospheric combustor. *J. Propul. Power* **32** (3), 628–645.

MCCULLOUGH, M., SMALL, M., STEMLER, T. & IU, H.H.C. 2015 Time lagged ordinal partition networks for capturing dynamics of continuous dynamical systems. *Chaos* **25** (5), 053101.

MEENA, M.G. & TAIRA, K. 2021 Identifying vortical network connectors for turbulent flow modification. *J. Fluid Mech.* **915**, A10.

MORGAN, C.J., SHIPLEY, K.J. & ANDERSON, W.E. 2015 Comparative evaluation between experiment and simulation for a transverse instability. *J. Propul. Power* **31** (6), 1696–1706.

MURAYAMA, S., KINUGAWA, H., TOKUDA, I.T. & GOTODA, H. 2018 Characterization and detection of thermoacoustic combustion oscillations based on statistical complexity and complex-network theory. *Phys. Rev.* E **97** (2), 022223.

MURUGESAN, M. & SUJITH, R.I. 2015 Combustion noise is scale-free: transition from scale-free to order at the onset of thermoacoustic instability. *J. Fluid Mech.* **772**, 225–245.

NEWMAN, M.E.J. 2004 Analysis of weighted networks. *Phys. Rev.* E **70** (5), 056131.

NEWMAN, M.E.J. 2006 Finding community structure in networks using the eigenvectors of matrices. *Phys. Rev.* E **74** (3), 036104.

NEWMAN, M.E.J. 2010 *Networks: An Introduction*. Oxford University Press.

O'CONNOR, J., ACHARYA, V. & LIEUWEN, T. 2015 Transverse combustion instabilities: acoustic, fluid mechanic, and flame processes. *Prog. Energy Combust. Sci.* **49**, 1–39.

OKUNO, Y., SMALL, M. & GOTODA, H. 2015 Dynamics of self-excited thermoacoustic instability in a combustion system: pseudo-periodic and high-dimensional nature. *Chaos* **25** (4), 043107.

REYNOLDS, D. 2009 *Gaussian Mixture Models*. Springer.

ROSSO, O.A., LARRONDO, H.A., MARTIN, M.T., PLASTINO, A. & FUENTES, M.A. 2007 Distinguishing noise from chaos. *Phys. Rev. Lett.* **99** (15), 154102.

SCHREIBER, T. 2000 Measuring information transfer. *Phys. Rev. Lett.* **85** (2), 461–464.

SHIMA, S., NAKAMURA, K., GOTODA, H., OHMICHI, Y. & MATSUYAMA, S. 2021 Formation mechanism of high-frequency combustion oscillations in a model rocket engine combustor. *Phys. Fluids* **33** (6), 064108.

SHINCHI, Y., TAKEDA, N., GOTODA, H., SHOJI, T. & YOSHIDA, S. 2021 Early detection of thermoacoustic combustion oscillations in staged multisector combustor. *AIAA J.* **59** (10), 4086–4093.

STANIEK, M. & LEHNERTZ, K. 2008 Symbolic transfer entropy. *Phys. Rev. Lett.* **100** (15), 158101.

SUJITH, R.I. & PAWAR, S.A. 2021 *Thermoacoustic Instability: A Complex Systems Perspective*. Springer.

SUJITH, R.I. & UNNI, V.R. 2020 Complex system approach to investigate and mitigate thermoacoustic instability in turbulent combustors. *Phys. Fluids* **32** (6), 061401.

https://doi.org/10.1017/jfm.2023.52 Published online by Cambridge University Press

SUJITH, R.I. & UNNI, V.R. 2021 Dynamical systems and complex systems theory to study unsteady combustion. *Proc. Combust. Inst.* **38** (3), 3445–3462.

TAIRA, K., NAIR, A.G. & BRUNTON, S.L. 2016 Network structure of two-dimensional decaying isotropic turbulence. *J. Fluid Mech.* **795**, R2.

URBANO, A., DOUASBIN, Q., SELLE, L., STAFFELBACH, G., CUENOT, B., SCHMITT, T., DUCRUIX, S. & CANDEL, S. 2017 Study of flame response to transverse acoustic modes from the LES of a 42-injector rocket engine. *Proc. Combust. Inst.* **36** (2), 2633–2639.

URBANO, A. & SELLE, L. 2017 Driving and damping mechanisms for transverse combustion instabilities in liquid rocket engines. *J. Fluid Mech.* **820**, R2.

URBANO, A., SELLE, L., STAFFELBACH, G., CUENOT, B., SCHMITT, T., DUCRUIX, S. & CANDEL, S. 2016 Exploration of combustion instability triggering using large eddy simulation of a multiple injector liquid rocket engine. *Combust. Flame* **169**, 129–140.

VAPNIK, V.N. 1999 An overview of statistical learning theory. *IEEE Trans. Neural Networks* **10** (5), 988–999.

VON LUXBURG, U. 2007 A tutorial on spectral clustering. *Stat. Comput.* **17** (4), 395–416.

WAXENEGGER-WILFING, G., SENGUPTA, U., MARTIN, J., ARMBRUSTER, W., HARDI, J., JUNIPER, M. & OSCHWALD, M. 2021 Early detection of thermoacoustic instabilities in a cryogenic rocket thrust chamber using combustion noise features and machine learning. *Chaos* **31** (6), 063128.

ZHANG, J. & SMALL, M. 2006 Complex network from pseudoperiodic time series: topology versus dynamics. *Phys. Rev. Lett.* **96** (23), 238701.

ZHANG, J., ZHOU, J., TANG, M., GUO, H., SMALL, M. & ZOU, Y. 2017 Constructing ordinal partition transition networks from multivariate time series. *Sci. Rep.* **7**, 7795.

https://doi.org/10.1017/jfm.2023.52 Published online by Cambridge University Press